Effective spinless fermions in the strong-coupling Kondo model

Winfried Koller,* Alexander Prüll, Hans Gerd Evertz, and Wolfgang von der Linden
Institut für Theoretische Physik, Technische Universität Graz, Petersgasse 16, A-8010 Graz, Austria
(Received 6 June 2002; published 31 October 2002)

Starting from the two-orbital Kondo-lattice model with classical t_{2g} spins, an effective spinless fermion model is derived for strong Hund coupling J_H with a projection technique. The model is studied by Monte Carlo simulations and analytically using a uniform hopping approximation. The results for the spinless fermion model are in remarkable agreement with those of the original Kondo-lattice model, independent of the carrier concentration, and even for moderate Hund coupling J_H. Phase separation, the phase diagram in uniform hopping approximation, as well as spectral properties including the formation of a pseudogap are discussed for both the Kondo-lattice and the effective spinless fermion model in one and three dimensions.

DOI: 10.1103/PhysRevB.66.144425 PACS number(s): 75.10.−b, 75.30.Kz, 71.10.−w

I. INTRODUCTION

The study of manganese oxides such as $La_{1-x}Sr_xMnO_3$ and $La_{1-x}Ca_xMnO_3$ has attracted considerable attention since the discovery of colossal magnetoresistance in these compounds.[1,2] These materials crystallize in the perovskite-type lattice structure where the crystal field partially lifts the degeneracy of the manganese d states. The energetically favorable threefold degenerate t_{2g} levels are populated with localized electrons, which according to Hund's rule form localized $S=3/2$ spins. The electronic configuration of the Mn^{3+} ions is $t_{2g}^3 e_g^1$, with one electron in the e_g orbital, which is missing in the Mn^{4+} ions. The e_g electrons can move between neighboring Mn ions mediated by bridging O^{2-} $2p$ orbitals. The interplay of electronic, spin, and orbital degrees of freedom along with the mutual interactions, such as the strong Hund coupling J_H of the itinerant electron to localized t_{2g} spins, Coulomb correlations, and electron-phonon coupling leads to a rich phase diagram including antiferromagnetic insulating, ferromagnetic metallic, and charge ordered domains.[3] Charge carriers moving in the spin and orbital background show interesting dynamical features.[4,5] The electronic degrees of freedom are generally treated by a Kondo-lattice model, which in the strong Hund coupling limit is commonly referred to as double-exchange (DE) model, a term first coined by Zener.[6]

Monte Carlo (MC) simulations have contributed significantly to our understanding of the manganites. Intense MC simulations for the DE model have been performed by Dagotto *et al.*[7] and Furukawa[8] in the space of the classically treated t_{2g} spins. Static and dynamical observables of the Kondo model have been determined.[9] These MC simulations gave first theoretical indications of phase separation (PS) (Ref. 10) in manganite models. Preliminary studies have been performed to analyze the importance of nearest-neighbor Coulomb repulsion in the two-orbital DE model[11] as well as the importance of classical phonons.[12]

Many publications are based on the $J_H=\infty$ limit. Here we propose an effective spinless fermion model for the strong-coupling limit of the Kondo-lattice Hamiltonian, which is equally simple as the $J_H=\infty$ limit but which still contains the crucial physical ingredients of finite J_H. The dynamic variables are e_g electrons with spins parallel to the t_{2g} spins at the respective sites. The influence of antiparallel spins is accounted for by the effective Hamiltonian. The derivation of the model is based on a projection technique, analogous to the derivation of the tJ model from the Hubbard model. The role of the Hubbard U is played by J_H which couples to the classical t_{2g} spins. In contrast to the tJ model, the high-energy subspace is thus controlled by classical variables, and consequently the resulting model is much simpler than the tJ model. For a given t_{2g} spin configuration, the resulting Hamiltonian is a *one-particle* operator. Its electronic trace can be evaluated analytically, once the one-particle energies are known, leading to an effective action for the t_{2g} spins, which can be simulated by Monte Carlo techniques.

The obvious advantage of this approach is the reduction of the dimension of the Hilbert space. This can be exploited in MC simulations by going to larger systems and/or additional degrees of freedom.

For a large range of parameters, the effective spinless fermion model is found to yield very satisfactory results and to perform much better than the rough $J_H\to\infty$ approximation. We compare spin and charge correlations as well as quasiparticle spectra of the projection approach with the full two-spin model and with the $J_H\to\infty$ limit.

The effective model is treated without approximations by Monte Carlo simulations as well as by a uniform hopping approximation (UHA) capturing the essential influence of the t_{2g} spins on the e_g electrons. The UHA computation can be performed analytically, particularly in the thermodynamic limit. Most of the UHA results are found to be in striking agreement with MC results. We find two-phase transitions as a function of the chemical potential, one close to the empty band and the second close to a completely filled band. At each phase transition we observe PS, as reported for the upper transition in Ref. 10. For a one-dimensional (1D) chain we derive an analytical expression for the two critical chemical potentials at which PS occurs.

For the 3D Kondo-lattice model, canonical UHA results yield a phase diagram that displays various types of antiferromagnetic (AF) order including spin canting, as well as ferromagnetism (FM). Our finite J_H results for 3D are in close agreement with those derived in the limit of infinite Hund coupling.[13] In the grand canonical ensemble we find, how-

ever, that only the 3D antiferromagnetic and the 3D ferromagnetic order prevail. The transition is again accompanied by PS.

The paper is organized as follows. In Sec. II the Kondo-lattice model is introduced. By applying a projection technique in Sec. III, this model is mapped onto the effective spinless fermion model. In Sec. IV we present the phase diagrams and phase-separation boundaries in one and three dimensions within a uniform hopping approximation. Results of Monte Carlo simulations for the original and the projected model are discussed in Sec. V. Finally, in Sec. VI we summarize the key conclusions.

II. MODEL HAMILTONIAN

In this paper, we will concentrate on purely electronic (t_{2g},e_g) properties, leaving phonon degrees of freedom for further studies. As proposed by Dagotto *et al.*[7] and Furukawa,[8] the t_{2g} spins $\mathbf{S}_i$ are treated classically, which is equivalent to the limit $S\to\infty$. The spin degrees of freedom are therefore replaced by unit vectors $\mathbf{S}_i$, parametrized by polar and azimuthal angles θ_i and ϕ_i, respectively, which represent the direction of the t_{2g} spin at lattice site $\mathbf{x}_i$. The magnitude of the spin is absorbed into the exchange couplings. It is expedient to use the individual t_{2g} spin directions as local quantization axes for the spin of the itinerant e_g electrons at the respective sites. This representation is particularly useful for the $J_H\to\infty$ limit, but also for the projection technique, which takes spin-flip processes for finite Hund coupling into account.

It is commonly believed that the electronic degrees of freedom are well described by a multiorbital Kondo-lattice model,

$$\hat{H}=-\sum_{i,j,\alpha,\beta,\sigma,\sigma'} t_{i\alpha,j\beta}^{\sigma,\sigma'} c_{i\alpha\sigma}^{\dagger} c_{j\beta\sigma'} + 2J_H \sum_{i\alpha} \hat{n}_{i\alpha\downarrow} + J' \sum_{\langle ij\rangle} \mathbf{S}_i\cdot\mathbf{S}_j . \tag{1}$$

It consists of a kinetic term with modified transfer integrals $t_{i\alpha,j\beta}^{\sigma,\sigma'}$, where $i(j)$ are site indices, $\alpha(\beta)$ orbital indices, and $\sigma(\sigma')$ are spin indices. The number of lattice sites will be denoted by L, and the number of orbitals per site by M. The operators $c_{i\alpha\sigma}^{\dagger}(c_{i\alpha\sigma})$ create (annihilate) e_g electrons at site x_i in the orbital α, with spin parallel $(\sigma=\uparrow)$ or antiparallel $(\sigma=\downarrow)$ to the local t_{2g} spin orientation $\mathbf{S}_i$. The next term describes the Hund coupling with exchange integral J_H. As usual, $\hat{n}_{i\alpha\sigma}$ is the spin-resolved occupation number operator. Usually, the Kondo-lattice Hamiltonian contains an additional term proportional to the electron number $\hat{N}_e$, $\hat{H}_c=-J_H\hat{N}_e$, which has been omitted in Eq. (1), as it merely results in a trivial shift of the chemical potential $\mu\to\mu-J_H$.

The modified hopping integrals $t_{i\alpha,j\beta}^{\sigma,\sigma'}$ depend upon the geometry of the e_g orbitals and the relative orientation of the t_{2g} spins:

$$t_{i\alpha,j\beta}^{\sigma,\sigma'}=t_{i\alpha,j\beta}u_{ij}^{\sigma,\sigma'} .$$

The first factor on the right-hand side is given by the hopping amplitudes $t_{i\alpha,j\beta}$, which read

$$t_{i,i+\hat{z}}=t\begin{pmatrix}0&0\\0&1\end{pmatrix},\quad t_{i,i+\hat{x}/\hat{y}}=t\begin{pmatrix}\frac{3}{4}&\mp\frac{\sqrt{3}}{4}\\ \mp\frac{\sqrt{3}}{4}&\frac{1}{4}\end{pmatrix} \tag{2}$$

as matrices in the orbital indices $\alpha,\beta=1(2)$, corresponding to the x^2-y^2 $(3z^2-r^2)$ orbitals (see, e.g., Ref. 1). The overall hopping strength is t, which will be used as a unit of energy, by setting $t=1$. The relative orientation of the t_{2g} spins at sites i and j enters via

$$u_{i,j}^{\sigma,\sigma}=c_ic_j+s_is_je^{i\sigma(\phi_j-\phi_i)},$$
$$u_{i,j}^{\sigma,-\sigma}=\sigma(c_is_je^{-i\sigma\phi_j}-c_js_ie^{-i\sigma\phi_i}), \tag{3}$$

with the abbreviations $c_j=\cos(\theta_j/2)$ and $s_j=\sin(\theta_j/2)$ and the restriction $0\leqslant\theta_j\leqslant\pi$. The modified hopping part of the Hamiltonian is still Hermitian, since $u_{i,j}^{\sigma,\sigma'}=(u_{j,i}^{\sigma',\sigma})^*$.

Finally, Eq. (1) contains a superexchange term. The value of the exchange coupling is $J'\approx 0.02$,[1] accounting for the weak antiferromagnetic coupling of the t_{2g} electrons. Here we will approximate the local t_{2g} spins classically. For strong Hund coupling $J_H\gg 1$, the electronic density of states (DOS) consists essentially of two subbands, a lower and an upper ''Kondo band,'' split by approximately $2J_H$. In the lower band, the itinerant e_g electrons move such that their spins are predominantly parallel to the t_{2g} spins, while the opposite is true for the upper band.[14] Throughout this paper, the electronic density n (number of electrons per site) will be restricted to $0\leqslant n\leqslant 1$, i.e., predominantly the lower Kondo band is involved.

III. PROJECTION TECHNIQUE

The separation of energy scales[15] is a well-known strategy to simplify quantum-mechanical many-body systems. In the case of manganites, the Hund coupling J_H is known to be much greater than the other parameters t and J'. Consequently, the hopping to antiparallel e_g-t_{2g} configurations can be treated in second-order perturbation theory[16,17] by a projection approach. On the low-energy scale, the dynamical variables are e_g electrons, with spin parallel to the local t_{2g} spins. The virtual excitations $(i\alpha\uparrow)\to(j\beta\downarrow)\to(i'\alpha'\uparrow)$, which are mediated by the hopping matrix, lead to an effective spinless fermion Hamiltonian

$$\hat{H}_p=-\sum_{i,j,\alpha,\beta} t_{i\alpha,j\beta}^{\uparrow\uparrow} c_{i\alpha}^{\dagger}c_{j\beta} - \sum_{i,\alpha,\alpha'}\left(\sum_{j,\beta}\frac{t_{i\alpha',j\beta}^{\uparrow\downarrow}t_{j\beta,i\alpha}^{\downarrow\uparrow}}{2J_H}\right)c_{i\alpha'}^{\dagger}c_{i\alpha} - \sum_{[i\neq i'],\alpha,\alpha'}\left(\sum_{j,\beta}\frac{t_{i'\alpha',j\beta}^{\uparrow\downarrow}t_{j\beta,i\alpha}^{\downarrow\uparrow}}{2J_H}\right)c_{i'\alpha'}^{\dagger}c_{i\alpha} + J'\sum_{\langle ij\rangle}\mathbf{S}_i\cdot\mathbf{S}_j . \tag{4}$$

The effective Hamiltonian contains the kinetic energy of e_g electrons, with spin parallel to the t_{2g} spins, (first term). The kinetic energy is optimized by aligning all t_{2g} spins, which is the usual ferromagnetic double-exchange effect. The second term describes an additional hybridization and favors antiferromagnetic t_{2g} spins leading to an effective antiferromagnetic interaction $J_{\rm eff}$, which is generally stronger than J'. The ''three-site'' hopping processes of the third term are of minor influence. We will see that this term is in general negligible. On the other hand, its inclusion does not really increase the numerical effort. Equation (4) is valid for arbitrary hopping matrices $t_{i\alpha,j\beta}$. In subsequent sections, however, the discussion will be restricted to nearest-neighbor hopping only.

The Hamiltonian Eq. (4) constitutes a spinless fermion model, similar to the one obtained in the $J_H\rightarrow\infty$ limit, which can be treated numerically along the lines proposed by Dagotto and co-workers[7] and Furukawa.[8] Finite J_H values can thus be treated with the same numerical effort as the case $J_H=\infty$. In the MC simulations, the weight for a t_{2g} spin configuration is determined by the grand canonical trace over the fermionic degrees of freedom in the one-electron potential created by the t_{2g} spins.

The obvious advantage of Eq. (4) as compared to Eq. (1) is the reduced Hilbert space.

IV. UNIFORM HOPPING APPROXIMATION

Before discussing approximation-free MC results for the effective spinless fermion model, we will investigate the main features of the Hamiltonian (4) by a uniform hopping approximation proposed by van den Brink and Khomskii.[13] To this end, we introduce two different mean angles between neighboring t_{2g} spins, one in z direction (θ_z) and one in the x-y plane (θ_{xy}). It should be stressed that θ_z and θ_{xy} are relative angles between adjacent spins, with values between 0 and π, and are not to be confused with the polar angles θ_i. We assume that these angles are the same between all neighboring spins, *i.e.*, $\mathbf{S}_i\cdot\mathbf{S}_{i\pm\hat{z}}=\cos\theta_z$ for all lattice sites i and $\mathbf{S}_i\cdot\mathbf{S}_{i\pm\hat{x}}=\mathbf{S}_i\cdot\mathbf{S}_{i\pm\hat{y}}=\cos\theta_{xy}$. The allowed spin configurations include, among others, ferromagnetism antiferromagnetism, as well as spin canted states. The impact of the t_{2g} spins on the hopping amplitudes simplifies to

$$u_z^{\sigma,\sigma}=\cos\left(\frac{\theta_z}{2}\right),\quad u_z^{\sigma,-\sigma}=\sin\left(\frac{\theta_z}{2}\right),$$

for hopping processes along the z direction, and similarly for $u_{xy}^{\sigma,\sigma'}$ for electron motion in the x-y plane. The hopping matrix is now translationally invariant. The inner product of the t_{2g} spins entering the superexchange reads

$$\mathbf{S}_i\cdot\mathbf{S}_{i+\hat{z}}=\cos\theta_z=2u_z^2-1,$$

and similarly for neighboring pairs in the x-y plane.

A. Phase separation in 1D systems

First we consider the simplest case, namely, a 1D chain in the z direction and we ignore the additional three-site hopping [third term in Eq. (4)]. At the end of this section we will show that it can indeed be neglected. Due to the symmetry of the hopping elements, the x^2-y^2 orbitals form an irrelevant dispersionless band, which will be ignored in the sequel. The influence of the average spin orientation is captured in the uniform hopping amplitude u. Assuming periodic boundary conditions, the Hamiltonian simplifies to

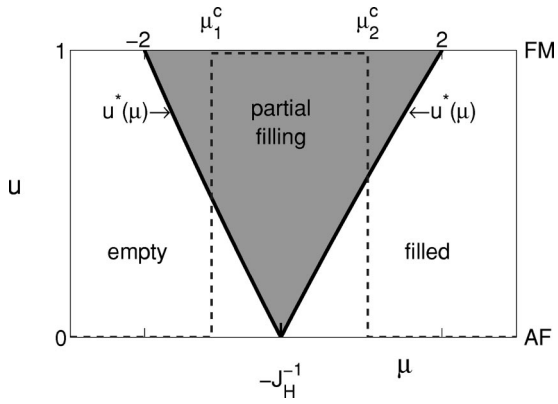

FIG. 1. Filling of the tight-binding band depending upon chemical potential and hopping amplitude. Condition for partial filling: $u>u^*(\mu)$. The minimum free-energy solution in UHA (dashed line) exhibits a jump (phase separation) from AF to FM order at μ_1^c and back to AF order at μ_2^c.

$$\hat{H}=-u\sum_{\langle ij\rangle}c_i^\dagger c_j-\frac{1-u^2}{J_H}\sum_i c_i^\dagger c_i+J'L(2u^2-1),\quad(5)$$

where we have dropped orbital indices. The virtual hopping processes couple merely to the density, and the dispersion of the spinless fermions is given by the shifted tight-binding band structure,

$$\epsilon_k=-2u\cos(k)-(1-u^2)/J_H.\quad(6)$$

The band width is $4u$. It vanishes accordingly for AF order, and reaches a maximum for FM order. In Fig. 1 the resulting band filling is schematically depicted for zero temperature as function of chemical potential and hopping amplitude. The condition for an empty/ filled band depends on the ''effective chemical potential''

$$\tilde{\mu}:=\left(\mu+\frac{1}{J_H}(1-u^2)\right)/u.\quad(7)$$

According to $\mu<\min_k(\epsilon_k)$, the band is empty if $\tilde{\mu}<-2$. For the completely filled band the condition reads $\tilde{\mu}>2$. Partial filling is possible for intermediate values of the chemical potential ($-2<\mu<2$) if the hopping amplitude exceeds a threshold $u^*(\mu)$. The logarithm of the grand canonical partition function reads

$$\ln Y=\sum_k\ln(1+e^{-\beta(\epsilon_k-\mu)})-\beta J'L(2u^2-1).$$

In the thermodynamic limit ($L\rightarrow\infty$) and for $T=0$, the free energy per lattice site is

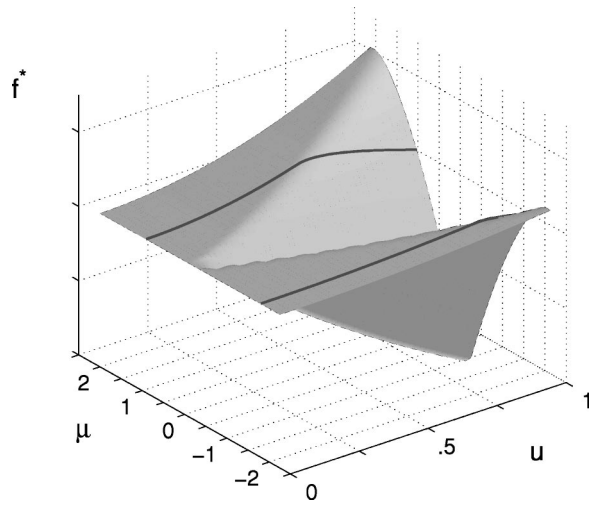

FIG. 2. Free energy as a function of chemical potential and hopping amplitude u for $T=0$, $J_H=6$, and $J'=0.02$. The solid lines are for μ_1^c and μ_2^c, respectively. For the sake of clarity, $f(u=0,\mu)$ has been subtracted.

$$f=uE(\tilde{\mu})-u\tilde{\mu}N(\tilde{\mu})+J'(2u^2-1), \tag{8}$$

with $E(x)$ being the mean kinetic energy and $N(x)$ the mean particle number of a tight-binding band with dispersion $-2\cos(k)$. For $|x|\leqslant 2$, these quantities are

$$E(x)=-\frac{\sqrt{4-x^2}}{\pi},\quad N(x)=\frac{1}{2}+\frac{\arcsin(x/2)}{\pi}.$$

The kinetic energy $E(x)$ is zero for the empty band ($x<-2$), as well as for the completely filled band ($x>2$). The mean particle number $N(x)$ is zero if the band is empty and unity if it is full. Figure 2 shows the free energy as a function of chemical potential and hopping amplitude u. We find local minima at $u=0$ (AF order) and $u=1$ (FM order). The kinetic terms decrease with increasing u, favoring FM order, while the t_{2g} spin energies increase with increasing u, favoring AF order. The global minimum switches from AF to FM at the critical chemical potential $\mu=\mu_1^c$ and back to AF at $\mu=\mu_2^c$. The values for the critical chemical potential follow from the condition $f|_{u=0}=f|_{u=1}$, yielding

$$(\mu^c+1/J_H)N_0(\mu^c)+2J'=\mu^cN(\mu^c)-E(\mu^c), \tag{9}$$

where $N_0(\mu^c)$ denotes the mean particle number for $u=0$, i.e., for perfect AF order. In this case, the tight-binding band is dispersionless and $N_0(\mu^c)$ is either 0 or 1, depending upon the actual value of the chemical potential.

For the standard parameter set $J_H=6$ and $J'=0.02$, the numerical values for μ^c are $\mu_1^c=-1.6730$ and $\mu_2^c=1.034\,31$.

The UHA solution corresponds to the global minimum of the free energy. Its location is depicted in Fig. 1 and the corresponding densities are shown as lines in Fig. 3. For large negative chemical potential the system is antiferromagnetic and the e_g band is empty. At μ_1^c, AFM domains with zero electron density coexist with FM domains with finite density n_1. Increasing μ leads to ferromagnetism, and the filling increases gradually with μ, following the tight-binding formula $n=\arccos(-\mu/2)/\pi$.

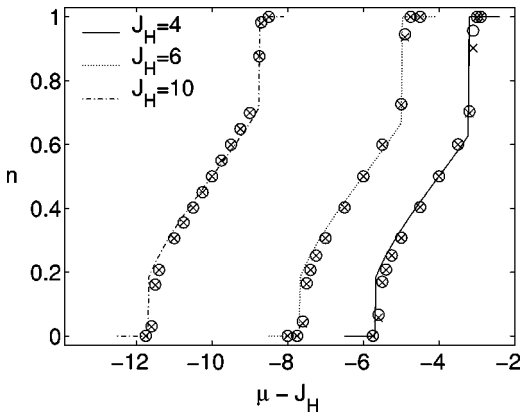

FIG. 3. Electron density versus chemical potential for $J_H=4,6$, and 10 (right to left), and $J'=0.02$. The lines correspond to UHA. MC results at $\beta=50$, $L=20$ for the spinless fermion model H_p (circles) are compared with those for the DE model H (crosses). Error bars of the MC data are smaller than the symbols.

At μ_2^c, FM domains with density $n_2>n_1$ coexist with AFM domains of density 1. Finally, for $\mu>\mu_2^c$, the system jumps back to antiferromagnetism, now at density 1. We thus see that the system exhibits phase separation. It should be pointed out that PS is suppressed if nearest-neighbor Coulomb repulsion among e_g electrons is included into the model.[18]

Let us now discuss the values of $\mu_{1,2}^c$ and the size of the discontinuity in n. According to Eq. (9), the first critical chemical potential $\mu_1^c=\mu^c(J')$, corresponding to $N_0(\mu)=0$, is independent of the actual value of J_H. Here the effective antiferromagnetic interaction J_{eff} purely stems from the superexchange coupling of the t_{2g} spins, $J_{\text{eff}}=J'$. This does, however, not mean that the Hund coupling is irrelevant for this phase transition. On the contrary, the phase transition is driven by the FM tendency introduced by the Hund coupling. The independence of J_H in our results means that there are no second-order corrections to the $J_H=\infty$ limit. The dependence of μ^c on J' is depicted in Fig. 4.

Now we turn to the second phase transition corresponding to $N_0(\mu^c)=1$. This transition is controlled by the stronger effective exchange coupling

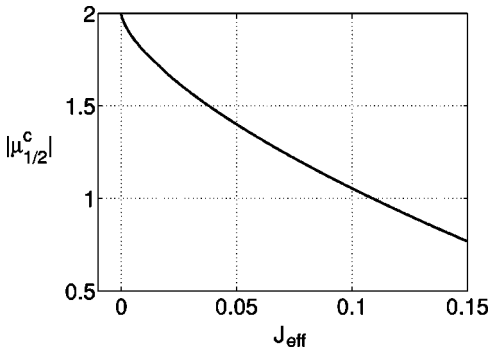

FIG. 4. Dependence of the critical chemical potential $|\mu_{1,2}^c|$ on the effective exchange coupling J_{eff}.

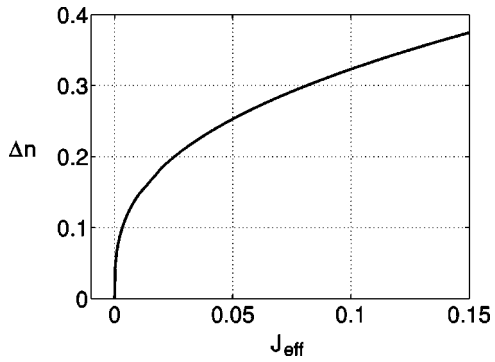

FIG. 5. Discontinuity in n as a function of the effective exchange coupling J_{eff}.

$$J_{\mathrm{eff}} = J' + \frac{1}{2J_H}, \tag{10}$$

as can be seen from Eq. (9), or directly from Eq. (5) at $N=1$. Due to the particle-hole relation $N(-\mu)+N(\mu)=1$, the second critical chemical potential is given by $\mu_2^c = -\mu^c(J_{\mathrm{eff}})$, depicted in Fig. 4. In the limit $J_H \to \infty$ we have $\mu_1^c = -\mu_2^c$. The density discontinuity is $\Delta n := N(\mu_1^c) = \Delta n(J')$ at μ_1^c and $\Delta n := 1 - N(\mu_2^c) = \Delta n(J_{\mathrm{eff}})$ at μ_2^c. It is depicted in Fig. 5. Series expansion of Eq. (9) with respect to μ^c about $\mu^c = -2$ yields $\Delta n = (3J'/\pi^2)^{1/3}$. At $J_{\mathrm{eff}}=0$ the slope of the curve diverges, implying that already an infinitesimal J_{eff} leads to phase separation in this regime.

For realistic parameter values ($J_H=6$ and $J'=0.02$) we find $\Delta n_1 \approx 0.18$ and $\Delta n_2 \approx 0.3$, respectively. The second value is mainly driven by the virtual hopping, which increases the tendency towards PS.

B. Impact of "three-site terms"

Here we consider the impact of the additional hopping in Eq. (4), which in the 1D case with one orbital results in a next-nearest neighbor hopping,

$$\hat{H}^* = -\frac{1-u^2}{2J_H} \sum_i c_{i+2}^\dagger c_i + \mathrm{H.c.}$$

Combined with the terms of Eq. (5), the resulting single-particle dispersion reads

$$\epsilon_k = -2u\cos k - \frac{1-u^2}{J_H} - \frac{1-u^2}{J_H}\cos(2k).$$

In the limit $u \to 1$, we recover the original tight-binding band. The density of states has additional van Hove singularities. Contrary to the dispersion of Eq. (5), the bandwidth remains finite in the limit $u \to 0$, due to $\hat{H}^*$.

Next we derive the conditions for phase separation. In the limit $T \to 0$, the free energy is given by

$$f = \int_{-\infty}^{\mu} d\epsilon \quad \rho_u(\epsilon)(\epsilon - \mu) - J'(2u^2 - 1),$$

where $\rho_u(\epsilon)$ denotes the density of states corresponding to ϵ_k. Numerical evaluation shows that the minima of f are still at $u=0$ and $u=1$. The condition for phase separation is therefore still $f|_{u=0} = f|_{u=1}$. In principle, due to the finite width of the band at $u=0$ intermediate particle numbers $N_0(\mu^c)$ are possible. A detailed calculation shows, however, that for realistic parameters, only $N_0(\mu^c)=0$ or $N_0(\mu^c)=1$ can meet the phase-separation criterion. For $N_0(\mu^c)=0$ and $N_0(\mu^c)=1$, however, no hopping is possible and consequently the additional hopping term vanishes. Therefore, the criterion for PS is the same as in Eq. (9) and the three-site hopping has no influence on the critical chemical potentials μ_c at which phase separation occurs.

In general, the modification of the bandwidth due to next-nearest neighbor hopping is small. It has almost negligible impact on the results. On the other hand it poses little extra-effort to include it in MC simulation.

C. Phase diagram in 3D systems

We now turn to the 3D case. In uniform hopping approximation, the superexchange reads

$$\hat{H}_{se} = J' L^3 [2(2u_{xy}^2 - 1) + (2u_z^2 - 1)],$$

where L denotes the linear dimensions of the system. Upon substituting uniform hopping amplitudes into Eq. (4), the fermionic part of the Hamiltonian can easily be diagonalized. The one-particle energies are given by the eigenvalues of a 2×2 matrix with matrix elements

$$\epsilon_{11}(k) = \frac{3}{2}[-u_{xy}(\cos k_x + \cos k_y) - (1-u_{xy}^2)/J_H],$$

$$\epsilon_{12}(k) = \frac{\sqrt{3}}{2} u_{xy}(\cos k_x - \cos k_y) = \epsilon_{21}(k), \tag{11}$$

$$\epsilon_{22}(k) = -2u_z \cos k_z - u_{xy}(\cos k_x + \cos k_y)/2 - [1 - u_z^2 + (1-u_{xy}^2)/4]/J_H$$

where the subscript 1 (2) refers to x^2-y^2 ($3z^2-r^2$) orbitals. The symmetry of the e_g wave function has been exploited in the above expressions. As a consequence of the UHA with two different angles θ_z and θ_{xy}, virtual hopping processes cannot induce transitions between different orbitals, and J_H appears only in the diagonal elements of the matrix.

We determine the phase diagram in the *canonical ensemble* at $T=0$ with respect to electron density n and exchange coupling J' for fixed Hund coupling $J_H=8$, with Eq. (11) evaluated on a 20^3 momentum lattice. For each parameter set, the free energy is minimized with respect to the hopping amplitudes. The resulting phase diagram is depicted in Fig. 6. At very low doping, 3D antiferromagnetic (G) order dominates, irrespective of the value of J', as long as $J' > 0$. Increasing the electron concentration for $J' > 0.02$, the system favors first a C phase, then an A phase, and finally ferromagnetism F. Similar results have been found for the $J_H = \infty$ limit.[13] Finite values for J_H have almost negligible influence on the phase diagram for densities $n < 0.5$. The G phase has not been reported in[13] since it has not been taken

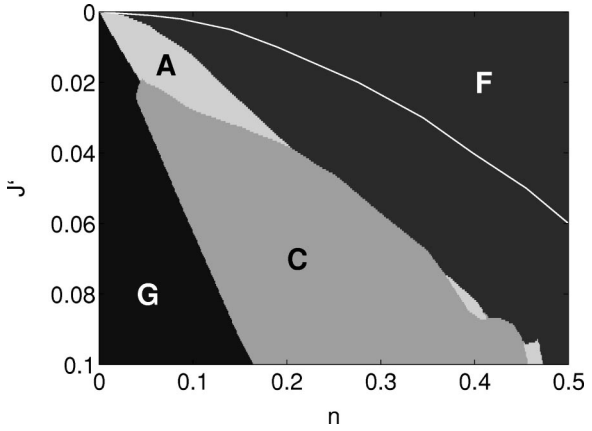

FIG. 6. Canonical $T=0$ UHA phase diagram of the spinless two-orbital Kondo-lattice model with classical t_{2g} spins for $J_H=8$. Depending upon the electron concentration of the canonical ensemble and the superexchange, *G* type, *A* type, *C* type antiferromagnetic phases or the ferromagnetic phase (*F*) are observed. Meaning of phases: $G=$(AF,AF); $A=$(FM,AF); $C=$(AF,FM); $F=$(FM,FM), where the first entry denotes the order in the *x*-*y* plane and the second in *z* direction. The solid line represents the phase boundary between *G* and *F* orders, respectively, obtained in a grand canonical ensemble.

into consideration. For small superexchange of the t_{2g} spins ($J'<0.018$), the transition from *G* to *A* phase evolves via spin canting. By increasing the electron doping, the *F* phase is reached without canting. The situation is more complex for larger values of *J'*. Figure 7 shows the optimal angles θ_z and θ_{xy} as a function of the electron density *n* for $J'=0.025$ and $J_H=8$. For $n<0.039$, there is 3D AF order (*G* type) with an increasing tendency towards canting between t_{2g} spins in the *x*-*y* plane. At $n\simeq 0.04$ this tendency is strongly reduced, while at the same time $\cos(\theta_z)$ discontinuously jumps to zero and we gradually enter the *C* phase by aligning the spins along the chains in *z* direction. The ferromagnetic chains are not perfectly antiferromagnetically stacked. At about 8% electron density we observe a phase transition to the *A* phase. At $n\approx 0.15$ an abrupt transition to 3D ferromagnetic order occurs.

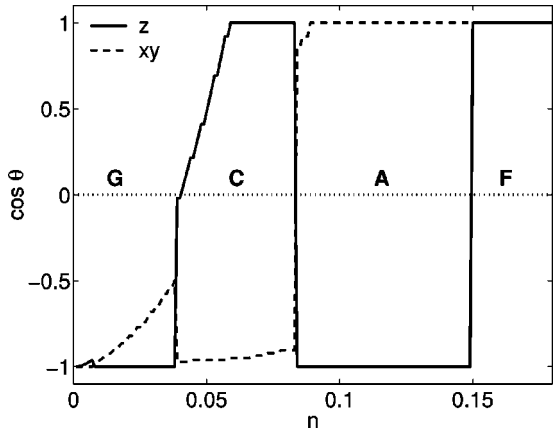

FIG. 7. Evolution of the optimal angles θ_z and θ_{xy} as function of the electron density *n* at $J'=0.025$, $J_H=8$. Further details same as Fig. 6.

Besides the analysis for the canonical ensemble, computations have been performed for the *grand canonical ensemble* as well. The results are significantly different. In the grand canonical ensemble, only the *G* and the *F* phases remain. The white solid line in Fig. 6 represents the phase boundary between the two phases. For fixed *J'*, the behavior is similar to that of the 1D system, depicted in Fig. 3. Below a critical chemical potential μ_1^c, the electron density is zero and the t_{2g} spins have AF order. At $\mu=\mu_1^c$, zero density and a finite density n_1, given by the solid line in Fig. 6, coexist. Concurrent with phase separation, AF and FM orders coexist. Above μ_1^c, the density increases monotonically. The second transition at μ_2^c is not shown in Fig. 6 as it occurs close to $n=1$. Therefore, the grand canonical UHA result does not exhibit the additional magnetic phases (*A* and *C*), which are observed in experiment. The relevant densities are never stabilized.

V. MC SIMULATIONS FOR 1D SYSTEMS

In this section we compare MC results, obtained for the original double exchange (DE) model (1), with those for the effective spinless fermion model [Eq. (4)], where the additional (''three-site'') hopping term has been neglected. We use the grand canonical Monte Carlo method introduced in Ref. 10 with open boundary conditions.

We restrict the discussion to 1D systems. There is no reason to believe that the performance of the approximation of effective spinless fermions is different in higher dimensions. Furthermore, the approximation has little influence on the orbital degrees of freedom, and we restrict the analysis to the one-orbital model. In all simulations, the superexchange coupling of the t_{2g} spins is $J'=0.02$.

Figure 3 shows the dependence of the electron density on the chemical potential. The system parameters are $L=20$, $\beta=50$, and J_H is varied between $J_H=4$ and $J_H=10$. All results for the two models are in almost perfect agreement. The ''largest'' difference can be observed at μ_2^c for $J_H=4$. The lines in Fig. 3 represent the results of the uniform hopping approximation, which are strikingly close to the MC data points. The discontinuities are more pronounced in UHA than in the MC data, which can partially be attributed to the fact that the UHA results are for $L=\infty$ and $T=0$. The treatment of finite temperatures in the UHA requires the determination of the number of t_{2g} configurations at a given *u* and is the subject of current investigations.[18]

The structure factor of the t_{2g} spins has been calculated for various densities *n* in the grand canonical ensemble by adjusting the chemical potential. The results are illustrated in Fig. 8. Again the data for the two models, the Kondo, and the effective spinless fermion model, are in perfect agreement within the error bars. Corroborating the UHA results of the preceding section, the filled band ($n=1$) has a peak at $k=\pi$, corresponding to AF order. For decreasing density the ferromagnetic peak increases up to $n=1/2$ and then it decreases again. The inset shows the nearest-neighbor and next-nearest-neighbor spin-correlation function versus density. We observe that both models yield the same magnetic

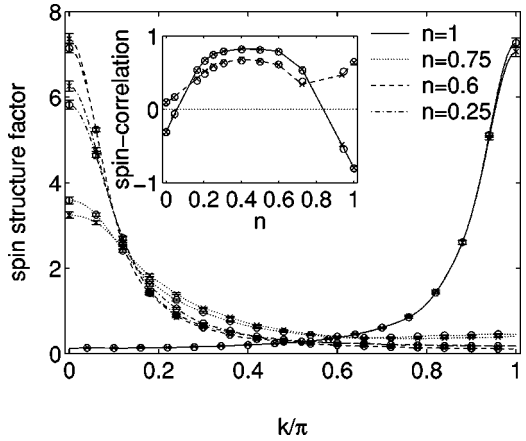

FIG. 8. Structure factor for the t_{2g} spins at various electron densities with $J_H=6$, $\beta=50$, and $L=20$, for the spinless fermion model H_p (circles), and for the DE model H (crosses). When not shown, error bars are smaller than the symbols. The inset shows the nearest-neighbor (solid line) and next-nearest-neighbor (dashed line) t_{2g} spin correlation.

behavior: AF order at low and high densities and a ferromagnetic phase at intermediate fillings. The pronounced peak at $k=\pi$ for $n=1$ results from (virtual) spin-flip processes, driven by the relatively strong exchange coupling $J_{\rm eff}=0.103$, Eq. (10). On the contrary the AF structure near $n=0$ is much less pronounced as it is merely driven by the weak super-exchange coupling $J'=0.02$. Figure 9 shows the structure factor for the t_{2g} spins at $n=1$ for different values of J_H. The AF peak decreases with increasing J_H and degenerates to a broad structure in the limit $J_H\rightarrow\infty$. Obviously, the inclusion of the second-order term to the effective spinless fermion model, which is missing in the commonly used $J_H=\infty$ limit, and which provides the strong exchange coupling $J_{\rm eff}$, is crucial for the correct description of the AF order at high electron density. The inset shows the spin structure for $n\approx 3/4$, at which the system exhibits ferromagnetic order. In this case, the FM correlations increase with increasing J_H.

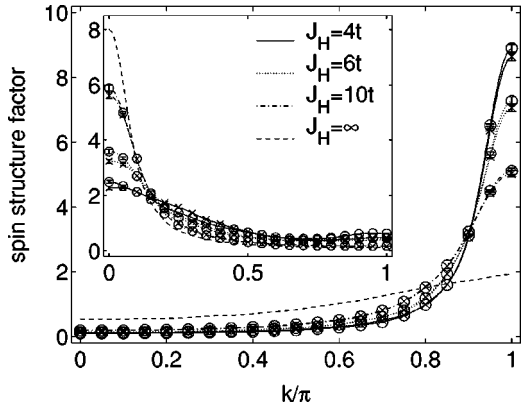

FIG. 9. Spin structure factor at $n=1$ (inset shows $n\approx 0.75$) for different values of J_H. Same symbols and parameters as in Fig. 8. In the limit $J_H\rightarrow\infty$ (dashed line), the intensity of the AF peak is considerably reduced.

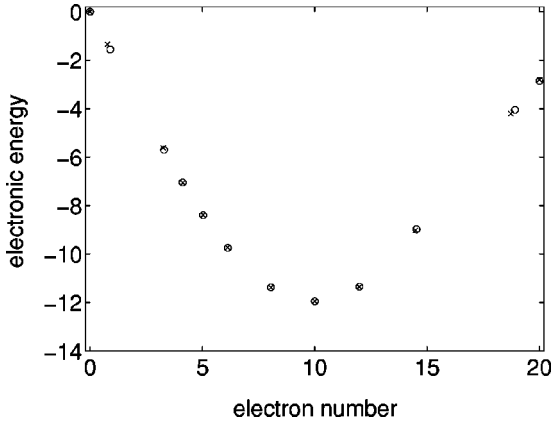

FIG. 10. Electronic contribution to the total energy versus electron number for $\beta=50$, $L=20$, and $J_H=6$. Results for the DE model $\hat{H}$ (crosses) are compared with those for the spinless fermion model $\hat{H}_p$ (circles).

As a further test for the spinless fermion model, the electronic contribution to the total energy is shown in Fig. 10. The energy for the Kondo-lattice model [first two terms in Eq. (1)] is compared with the corresponding contributions in the effective spinless fermion model [Eq. (4)]. For all fillings the results are in very good agreement.

Quantitatively, the largest differences are found for $n=1$. For this density the dependence of the energy on J_H is studied in Fig. 11. A detailed comparison reveals that the effective model describes the electronic energy extremely well, even in the moderate coupling regime. The ubiquitous $J_H=\infty$ approximation, on the other hand, yields zero electronic energy. For the parameters underlying Fig. 11, the t_{2g} spins are antiferromagnetically ordered and the lower Kondo band, or rather the single band of the spinless fermion model, is completely filled. Nevertheless, the kinetic electronic energy is finite due to (virtual) spin-flip processes. It should be pointed out that the additional (three-site) hopping term in Eq. (4) has no influence on this result as the band is entirely filled.

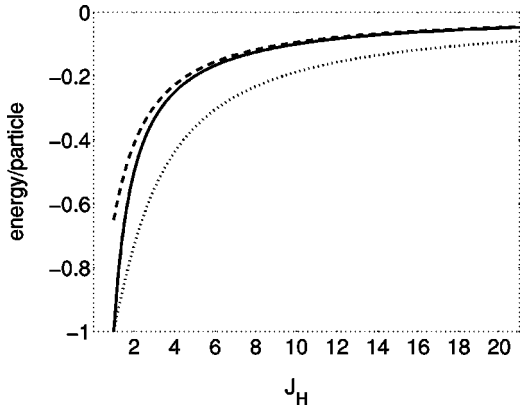

FIG. 11. Electronic energies versus Hund coupling J_H for a completely filled 20-site chain at $T=0$. Kinetic energy (dotted line) and total electronic energy (dashed lines) for the Kondo-lattice model. The solid line represents the total electronic energy for the effective spinless fermion model.

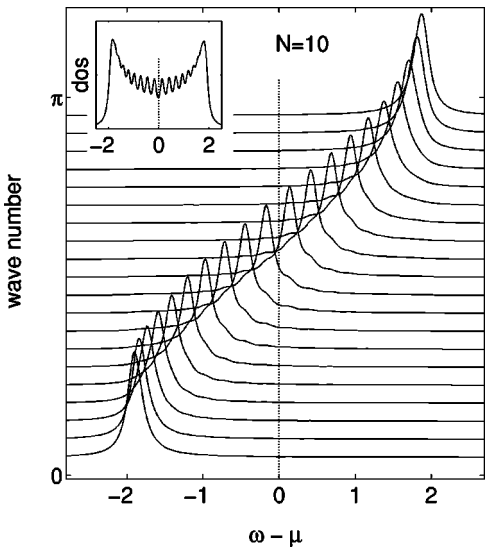

FIG. 12. Spectral function obtained by a grand canonical simulation for $n=1/2$ with $J_H=6$, $L=20$, and $\beta=50$. An intrinsic linewidth $\gamma=0.1$ has been added. The results for the Kondo model and the effective spinless fermion model are indistinguishable.

Next we study the spectral function $A_k(\omega)$ in the grand canonical ensemble for various mean electron densities covering the regimes for AF and FM order, as well as phase separation. In all cases the system geometry is a 20-site chain with open boundary conditions at inverse temperature $\beta=50$, and exchange couplings $J'=0.02$ and $J_H=6$. We start out with the spectra in Fig. 12 for strong FM order at a mean particle density of $n=1/2$. According to the inset of Fig. 8, the spin correlations are 0.82 and 0.67 for nearest- and next-nearest neighbors, respectively. The spectral function depicted in Fig. 12 resembles closely that of a tight-binding model, valid for perfect FM order. The bandwidth is slightly reduced, and for k values close to the Fermi momentum, $A_k(\omega)$ exhibits some minor shoulders. The half width at half maximum of the peaks agrees with γ, the value by which the finite-size δ peaks have been broadened. The inset displays the DOS, which agrees with the tight-binding density of states for open boundary conditions. Next we increase the mean density to $n=0.75$, corresponding to a chemical potential close to μ_2^c. The spin order is still predominantly ferromagnetic. The results in Fig. 13 show that both models yield very similar results, namely, a tight-binding type of quasiparticle band. The spectral peaks are, however, significantly broader than the mock width γ, and upon approaching the Fermi momentum the width increases asymmetrically towards the fermi level. The origin of the broad structures are the random deviations of the t_{2g} spins from perfect FM order. The resulting density of states has piled up spectral weight in the center and reveals a precursor of a pseudogap at the Fermi energy. Interestingly, the DOS is almost center symmetric and a mirror image of the ''pseudo-gap'' occurs also at the lower band edge.

The next panel depicts results for $n=0.95$, correspond to a chemical potential slightly above μ_{c2}, where the spin order

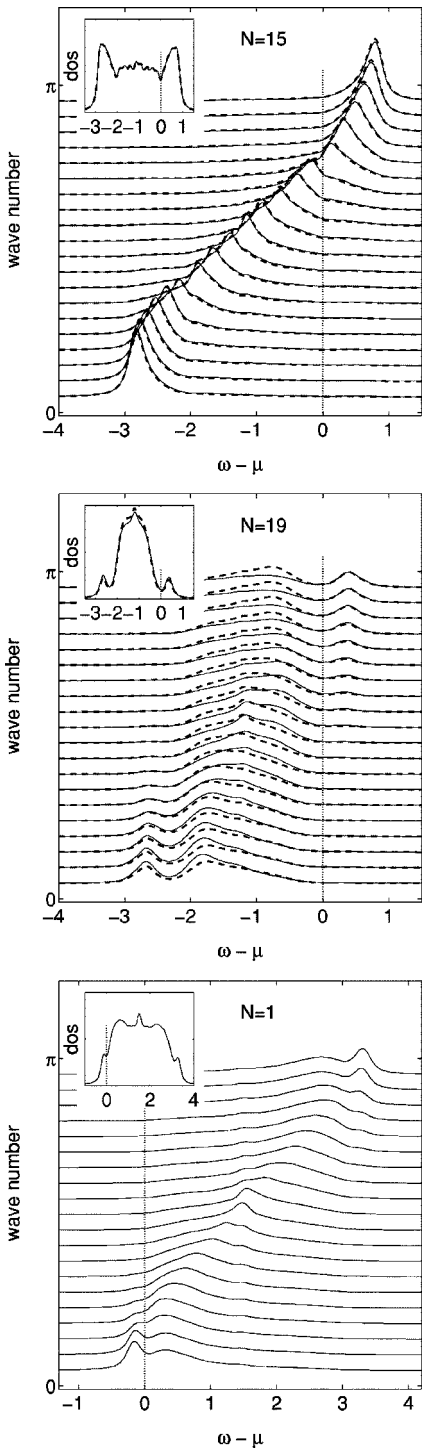

FIG. 13. Same as Fig. 12. The indicated particle numbers correspond to $n=0.75$, $n=0.95$, and $n=0.05$. Results for the Kondo model are represented by solid lines, and those for the effective spinless fermion model by dashed lines.

is predominantly antiferromagnetic. Now the pseudo-gap, as discussed by Moreo *et al.*,[19] is clearly visible. Additionally we observe a ''mirror pseudogap'' at the lower band edge. There is still good qualitative agreement between the results of the two models. Quantitatively, however, there are deviations in the structures below the pseudogap. The density of states is still remarkably well described by the spinless fer-

mion model.

In the opposite limit of low carrier concentration ($n=0.05$), the chemical potential is close to μ_{c1}, where we find similar features. Again, together with the coexistence of FM and AFM order, a pseudogap shows up at the chemical potential as well as at the upper band edge. The pseudo-gap is less pronounced in this case, where the antiferromagnetic exchange coupling J' is much smaller than J_{eff} at μ_2^c.

In both models a considerable amount of spectral weight is transferred from the band edges to the center. Interestingly, the density of states is almost center symmetric. The pseudogap is present in the spectral function irrespective of the wave vector *k*. Moreo *et al*. argued that the pseudogap is formed due to the presence of mixed phases with irregular formations of FM domains. In contrast to this interpretation, we find the pseudogap also in the perfect AF regime with a single electron (hole).

Generally we observe, in agreement with angle-resolved photoemission fine-structure spectroscopy (ARPES) experiments,[20] that the width of peaks increases towards the Fermi energy and the spectral intensity decreases since spectral weight is transferred to the unoccupied part of the spectrum, which is not visible in ARPES. Furthermore, the peaks are generally much broader than the experimental resolution.

VI. CONCLUSIONS

We have developed an effective spinless fermion model for the strong-coupling multi-orbital Kondo-lattice model. The effective model has a reduced Hilbert space, and is particularly suitable for MC simulations. The numerical complexity is the same as that of the $J_H=\infty$ model. The reduced Hilbert space allows one to study higher spatial dimensions and/or additional degrees of freedom, such as phonons.

Based on the evaluation of various observables, the effective spinless fermion model performs strikingly well, even for moderate Hund coupling.

It appears that virtual spin-flip processes included in our approach, which are missing in the $J_H=\infty$ model, are crucial for the antiferromagnetic phase close to half filling ($n=1$), where they provide a strong effective exchange coupling $J_{\text{eff}}=J'+1/(2J_H)$.

Two phase transitions from AF to FM order and vice versa are observed, accompanied by phase separation. Analytic expressions for the chemical potential at which phase separation occurs in a 1D chain have been derived in uniform hopping approximation (UHA). It has been shown, however, that they are in extremely good agreement with approximation-free MC results.

The UHA phase diagram of the 3D spinless fermion model has been determined. In canonical ensembles, the magnetic phase diagram is in qualitative agreement with that obtained in previous studies for the $J_H=\infty$ limit. Experimentally observed phases, such as *G*, *A*, *C*, and *F* orders are found. On the other hand, grand canonical ensemble calculations show that only 3D AF and 3D FM orders prevail. The transition between the two phases is accompanied by phase separation. Densities, required for other phases, are not stable in UHA.

The spectral functions show a remarkable center symmetry. In the AF phase, at low and high electron densities, a pseudogap structure is observed at the chemical potential and a mirror image at the opposite edge of the spectrum.

In passing, it should be noted that nearest-neighbor Coulomb repulsion of the e_g electrons in a two-orbital model can be detrimental for phase separation. Detailed results will be discussed elsewhere.[18]

ACKNOWLEDGMENT

This work was partially supported by the Austrian Science Fund (FWF), Project No. P15834-PHY.

*Electronic address: koller@itp.tu-graz.ac.at

[1] E. Dagotto, T. Hotta, and A. Moreo, Phys. Rep. **344**, 1 (2001).

[2] A.M. Oleś, M. Cuoco, and N.B. Perkins, in *Lectures on the Physics of Highly Correlated Electron Systems IV*, edited by Ferdinando Marcini, AIP Conf. Proc. No. 527 (AIP, Melville, NY, 2000), pp. 226–380.

[3] T. Kaplan and S. Mahanti, *Physics of Manganites*, 1st ed. (Kluwer Academic/Plenum Publishers, New York/Boston, 1998).

[4] P. Horsch, J. Jaklic, and F. Mack, Phys. Rev. B **59**, R14 149 (1999).

[5] J. Bala, A.M. Oles, and P. Horsch, Phys. Rev. B **65**, 134420 (2002).

[6] C. Zener, Phys. Rev. **82**, 403 (1951).

[7] E. Dagotto, S. Yunoki, A.L. Malvezzi, A. Moreo, J. Hu, S. Capponi, D. Poilblanc, and N. Furukawa, Phys. Rev. B **58**, 6414 (1998).

[8] N. Furukawa, *Physics of Manganites*, 1st ed. (Kluwer Academic Publisher, New York, 1998).

[9] S. Yunoki and A. Moreo, Phys. Rev. B **58**, 6403 (1998).

[10] S. Yunoki, J. Hu, A.L. Malvezzi, A. Moreo, N. Furukawa, and E. Dagotto, Phys. Rev. Lett. **80**, 845 (1998).

[11] T. Hotta, A.L. Malvezzi, and E. Dagotto, Phys. Rev. B **62**, 9432 (2000).

[12] S. Yunoki, A. Moreo, and E. Dagotto, Phys. Rev. Lett. **81**, 5612 (1998).

[13] J. van den Brink and D. Khomskii, Phys. Rev. Lett. **82**, 1016 (1999).

[14] W. von der Linden and W. Nolting, Z. Phys. B: Condens. Matter **48**, 191 (1982).

[15] A. Auerbach, *Interacting Electrons and Quantum Magnetism*, 1st ed. (Springer-Verlag, New York, 1994).

[16] S. Yarlagadda and C.S. Ting, Int. J. Mod. Phys. B **15**, 2719 (2001).

[17] S.-Q. Shen and Z.D. Wang, Phys. Rev. B **61**, 9532 (2000).
[18] W. Koller, A. Prüll, H.G. Evertz, and W. von der Linden (unpublished).
[19] A. Moreo, S. Yunoki, and E. Dagotto, Phys. Rev. Lett. **83**, 2773 (1999).
[20] D.S. Dessau, T. Saitoh, C.H. Park, Z.X. Shen, P. Villella, N. Hamada, Y. Moritomo, and Y. Tokura, Phys. Rev. Lett. **81**, 192 (1998).